

Co-Doped Rare-Earth (La, Pr) and Co-Al Substituted M-Type Strontium Hexaferrite: Structural, Magnetic, and Mossbauer Spectroscopy Study

Madhav L. Ghimire^{1,2*}, Dom L. Kunwar³, Jiba N. Dahal⁴, Dipesh Neupane¹, Sunghyun Yoon⁵, Sanjay R. Mishra¹

¹Department of Physics and Materials Science, The University of Memphis, Memphis, TN, USA

²Department of Physics, Virginia Commonwealth University, Richmond, VA, USA

³Department of Physics, Kent State University, Kent, OH, USA

⁴Department of Physics and Astronomy, Truman State University, Kirksville, MO, USA

⁵Department of Physics, Gunsan National University, Gunsan, South Korea

Email: *ghimirem@vcu.edu, madhav.ghim@gmail.com

How to cite this paper: Ghimire, M.L., Kunwar, D.L., Dahal, J.N., Neupane, D., Yoon, S. and Mishra, S.R. (2020) Co-Doped Rare-Earth (La, Pr) and Co-Al Substituted M-Type Strontium Hexaferrite: Structural, Magnetic, and Mossbauer Spectroscopy Study. *Materials Sciences and Applications*, 11, 474-493.

<https://doi.org/10.4236/msa.2020.117033>

Received: June 5, 2020

Accepted: July 17, 2020

Published: July 20, 2020

Copyright © 2020 by author(s) and Scientific Research Publishing Inc. This work is licensed under the Creative Commons Attribution International License (CC BY 4.0).

<http://creativecommons.org/licenses/by/4.0/>



Open Access

Abstract

The present study investigates the influence of La³⁺ and Pr³⁺ doping on the structural, magnetic properties, and hyperfine fields of Sr_{0.7}RE_{0.3}Fe_{12-2x}Co_xAl_xO₁₉, (RE: La³⁺ and Pr³⁺, $x = 0.0 - 0.8$) hexaferrite compounds prepared via auto-combustion technique. The XRD analysis shows a linear decrease in a and c lattice and unit cell volume contraction with the content x . The room temperature magnetic study shows that for the Pr³⁺ doped Sr_{0.7}Pr_{0.3}Fe_{12-2x}Co_xAl_xO₁₉ (Pr³⁺-SrM), the magnetization value monotonically decreases while for La³⁺ doped Sr_{0.7}La_{0.3}Fe_{12-2x}Co_xAl_xO₁₉ (La³⁺-SrM) magnetization value shows a noticeable increase in magnetization value with x . The coercivity of the Pr³⁺-SrM compound was observed to decrease while that of the La³⁺-SrM compound showed a marked 40% increase at $x = 0.2$ (~5829 Oe) in comparison to undoped SrFe₁₂O₁₉ (~3918 Oe). A difference in Curie temperature was also observed, with $T_c \sim 525^\circ\text{C}$ at $x = 0.4$ for Pr³⁺-SrM and $T_c = 505^\circ\text{C}$ for $x = 0.4$ for La³⁺-SrM compound. The observed differences in magnetic properties have been explained on the basis of the site occupancy of Co²⁺ and Al³⁺ in the presence of rare-earth ions. The presence of non-magnetic rare-earth ion, La³⁺, improved saturation magnetization, and coercivity and deemed suitable replacement for Sr²⁺. The hyperfine parameters namely quadrupole shift showed a decrease with the La³⁺ or Pr³⁺ doping independent of (Co²⁺-Al³⁺) ions doping. Overall, the Mossbauer analysis suggests that the (Co²⁺-Al³⁺) impurities prefer occupancy at $2a$ site.

Keywords

Doped Hexaferrite, M-Type Hexaferrite, X-Ray Diffraction, Mossbauer Spectroscopy

1. Introduction

The M-type hexaferrite, Strontium hexaferrite, is an excellent candidate for technological applications because of its high uniaxial magneto-crystalline anisotropy, large magnetization, high permeability, low conductive losses, excellent chemical stability, corrosion resistance and excellent high-frequency response [1] [2] [3]. Strontium hexaferrite has been widely used as materials for industrial applications, such as in microwave devices, small motors, electromagnetic wave absorber, and ferroxdures [4] [5]. Besides this, the popularity of strontium hexaferrite is also due to its economic success, which is its low price per unit available magnetic energy and its wide availability. So far, efforts have been made to further improve electrical, dielectric and magnetic properties of strontium hexaferrite by means of doping, heat treatment, ion substitution, and processing conditions [6] [7] [8] [9] [10].

In M-type hexaferrite, the structure is comprised of 64 ions per hexagonal unit cell on 11 distinct basis sites. The 24 Fe^{3+} iron atoms of a unit cell occupy five different interstitial sites: three octahedral sites ($2a$, $12k$ and $4f_2$), one tetrahedral site ($4f_1$) and one trigonal bi-pyramidal site ($2b$). The coupling of these sites by superexchange interaction via O_2^- gives rise to a ferrimagnetic structure. The sites $12k$, $2a$, and $2b$ are sites with spin up while sites $4f_2$ and $4f_1$ are sites with the down-spin [10]. This provides an ample opportunity to tune the magnetic properties of M-type hexaferrite compound by carefully engineering site occupancy in favor of increasing net magnetization of the compound. In view of this, attempts are made with either partial substitution of Sr^{2+} or Fe^{3+} sites. For example, substitution with non-magnetic ions such as Al^{3+} [11] [12], Zn^{3+} [13], Ga^{3+} [14] and Cd^{3+} [15] [16] and magnetic ions such as Co^{2+} [17] and Cr^{3+} [18] at Fe sites, or with the partial substitution of Sr^{2+} site by RE^{3+} such as La^{3+} [19] [20], Nd^{3+} [21], Sm^{3+} [22] [23] and Pr^{3+} [24] ions, and substitution of $\text{Sr}^{2+}/\text{Fe}^{3+}$ together with Pr-Zn [25], La-Cu [26], and La-Zn [27]. The majority of these studies have attributed changes in the magnetic behavior of doped SrM either to the site-occupancy, which perturbs exchange interaction between $\text{Fe}^{3+}-\text{O}^{2-}-\text{Fe}^{3+}$, anisotropy changes occurring at $2b$ sites due to perturbation in electric field gradient or extrinsic features such as particle size.

Doping of non-magnetic Al^{3+} in $\text{SrFe}_{12-x}\text{Al}_x\text{O}_{19}$ has been reported to bring a considerable enhancement in the coercivity along with a reduction in saturation magnetization [11] [28] [29]. Thus with the Al^{3+} substitution, in spite of a large increase in the coercivity, the compound attains abysmal magnetization value. A strategy could be designed to keep both coercivity and magnetization value high.

In the present work, an attempt is made to co-doped Co^{2+} - Al^{3+} in the $\text{SrFe}_{12}\text{O}_{19}$ compound. Magnetic ion Co^{2+} ($\sim 3.7 \mu_B$) is chosen to maintain high magnetization value, while Al^{3+} doping is expected to maintain high coercivity value in $\text{SrFe}_{12}\text{O}_{19}$. Furthermore, Lechevallier *et al.* reported that the only light rare-earth enters the structure, which a solubility that is related to the shape of the charge distribution of the $4f$ electrons to its surroundings in the crystal structure. Thus, only those rare-earth ions have easy accommodation at the Sr^{2+} site, whose surroundings favor an oblate electronic distribution. This makes Pr and Nd (with oblate $4f$ charge distribution, negative Stevens constant) ideal candidate to occupy the Sr^{2+} site [25]. Furthermore, Co^{2+} ions were reported to modify the surroundings of the Sr^{2+} site, improving the introduction of rare-earth ions with oblate electronic distributions, in fact, the presence of Co^{2+} increases the solubility of Pr^{3+} [25]. Also, RE^{3+} - Co^{2+} - Al^{3+} , co-substitution naturally maintains the charge neutrality condition in the compound. With the substitution of RE^{3+} for the Sr^{2+} , the extra positive charge is compensated by the substitution of Co^{2+} at the Fe^{3+} site. In the absence of Co^{2+} , one of the Fe^{3+} has to convert to Fe^{2+} , which has a deleterious effect on the magnetization. With this strategy in mind, the present study investigates, the influence of the 1) rare-earth substitution, Pr^{3+} , and La^{3+} , at the Sr^{2+} site and 2) Co^{2+} - Al^{3+} substitution at Fe^{3+} sites on the overall magnetic properties of the $\text{Sr}_{0.7}\text{RE}_{0.3}\text{Fe}_{12-2x}\text{Co}_x\text{Al}_x\text{O}_{19}$ compound.

2. Experimental

The series of $\text{Sr}_{0.7}\text{RE}_{0.3}\text{Fe}_{12-2x}\text{Co}_x\text{Al}_x\text{O}_{19}$ (RE: La^{3+} and Pr^{3+} , $x = 0, 0.2, 0.4, 0.6$ and 0.8) compounds were prepared by auto-combustion method [11]. Nitrate salts of $\text{Fe}(\text{NO}_3)_3 \cdot 9\text{H}_2\text{O}$ (Sigma Aldrich, 99%), $\text{Sr}(\text{NO}_3)_2$ (Sigma Aldrich, 99%), $\text{Al}(\text{NO}_3)_3 \cdot 9\text{H}_2\text{O}$ (Sigma Aldrich, 99%), $\text{RE}(\text{NO}_3)_3 \cdot 9\text{H}_2\text{O}$ (Sigma Aldrich, 99%) and $\text{C}_6\text{H}_8\text{O}_7$ (Sigma Aldrich, 99%) were selected for the synthesis $\text{Sr}_{0.7}\text{RE}_{0.3}\text{Fe}_{12-2x}\text{Co}_x\text{Al}_x\text{O}_{19}$ compounds. The stoichiometric amount of nitrates salts and citric acid were mixed in 25 ml of deionized water under constant stirring on a hot plate at 80°C for about 30 minutes. Aqueous ammonia was added dropwise in the homogeneous mixture until the pH value of the solution reached 6.5. The intermediate precipitate was heated at 100°C on a hot plate under stirring until the viscous brown gel is formed. The temperature is suddenly increased to 300°C to turn it into magnetic powder. Powders were calcined in air at 1000°C for twelve hours. The precursor used in the preparation of 1 g of sample is listed in **Table 1**.

The crystal structure and phase purity of the obtained samples were identified by analyzing x -ray diffraction (XRD) pattern collected via Bruker D8 Advance X-ray diffractometer using Cu K_α radiation source ($\lambda \sim 0.154056 \text{ nm}$). Vibrating sample magnetometer (VSM) was used to collect hysteresis loops of the samples at room temperature in the maximum field of 1.2 T. Curie temperature, T_C , were measured using Thermogravimetric analyzer, TGA, (DuPont 910) equipped with a permanent magnet. Room temperature ^{57}Fe Mossbauer spectroscopy was

Table 1. Stoichiometry weight of of SrFe₁₂O₁₉, Sr_{0.7}La_{0.3}Fe_{12-2x}Co_xAl_xO₁₉ and Sr_{0.7}Pr_{0.3}Fe_{12-2x}Co_xAl_xO₁₉.

	Mass (g)					
	Sr(NO ₃) ₂	La(NO ₃) ₂ ·6H ₂ O	Fe(NO ₃) ₂ ·9H ₂ O	Co(NO ₃) ₂ ·6H ₂ O	Al(NO ₃) ₂ ·9H ₂ O	Citric acid
SrFe ₁₂ O ₁₉	0.199	0.000	4.567	0.000	0.000	2.573
Sr_{0.7}La_{0.3}Fe_{12-2x}Co_xAl_xO₁₉						
<i>x</i> = 0.0	0.176	0.361	4.038	0.000	0.000	2.275
<i>x</i> = 0.2	0.175	0.359	3.951	0.048	0.062	2.264
<i>x</i> = 0.4	0.175	0.357	3.865	0.096	0.124	2.253
<i>x</i> = 0.6	0.174	0.355	3.780	0.143	0.185	2.241
<i>x</i> = 0.8	0.173	0.354	3.695	0.190	0.245	2.230
Sr_{0.7}Pr_{0.3}Fe_{12-2x}Co_xAl_xO₁₉						
		Pr(NO ₃) ₂ ·6H ₂ O				
<i>x</i> = 0.0	0.137	0.125	4.499	0.000	0.000	2.535
<i>x</i> = 0.2	0.137	0.124	4.400	0.054	0.069	2.521
<i>x</i> = 0.4	0.136	0.123	4.301	0.107	0.138	2.507
<i>x</i> = 0.6	0.135	0.123	4.204	0.159	0.205	2.493
<i>x</i> = 0.8	0.134	0.122	4.107	0.211	0.272	2.480

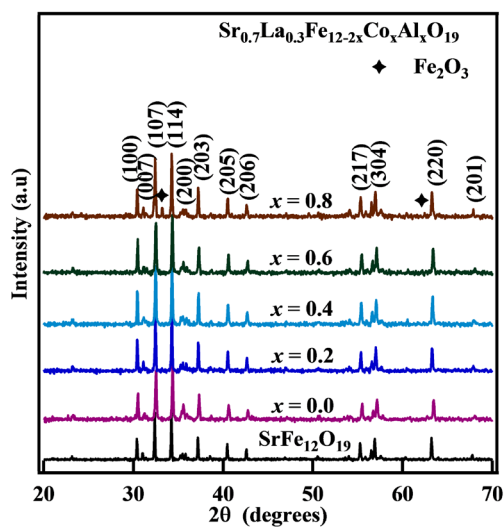
employed to derive hyperfine parameters. The Mossbauer spectrometer (SEE Co. Minneapolis, MN USA) was calibrated against α -Fe foil. The Mossbauer spectra were analyzed using WMOSS software (SEE Co. Minneapolis, MN USA).

3. Results and Discussions

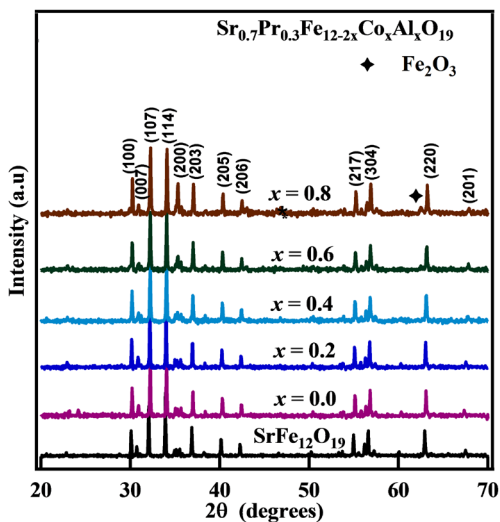
The room temperature XRD pattern of Sr_{0.7}RE_{0.3}Fe_{12-2x}Co_xAl_xO₁₉ (RE: La³⁺ and Pr³⁺, *x* = 0.0, 0.2, 0.4, 0.6, and 0.8) is shown in **Figure 1**. XRD patterns of the substituted compounds indicated the presence of a magnetoplumbite structure (ICCD 080-1198) corresponding to the hexagonal P63/mmc symmetry phase group without any secondary phase. The lattice parameters of the compound were calculated from their inter-planar spacing d_{hkl} corresponding to the major peaks (107), (114), and (008) using equation [30]:

$$d_{(hkl)} = \left(\frac{4(h^2 + hk + k^2)}{3a^2} + \frac{l^2}{c^2} \right)^{\frac{1}{2}} \quad (1)$$

where *h*, *k*, and *l* are Miller indices. The calculated lattice parameters *a* and *c* of the hexaferrites are shown in **Table 2**. The plot for *a* and *c* as a function of doping content is shown in **Figure 2**. A linear decrease in the lattice parameters *a* and *c* with the doping content was observed. The linear decrease in the lattice parameter may occur due to the substitution of Al³⁺ (ionic radii, *r* ~ 0.51 Å) and



(a)



(b)

Figure 1. X-ray diffraction pattern of (a) $\text{Sr}_{0.7}\text{La}_{0.3}\text{Fe}_{12-2x}\text{Co}_x\text{Al}_x\text{O}_{19}$ and (b) $\text{Sr}_{0.7}\text{Pr}_{0.3}\text{Fe}_{12-2x}\text{Co}_x\text{Al}_x\text{O}_{19}$ obtained using Cu K α radiation.

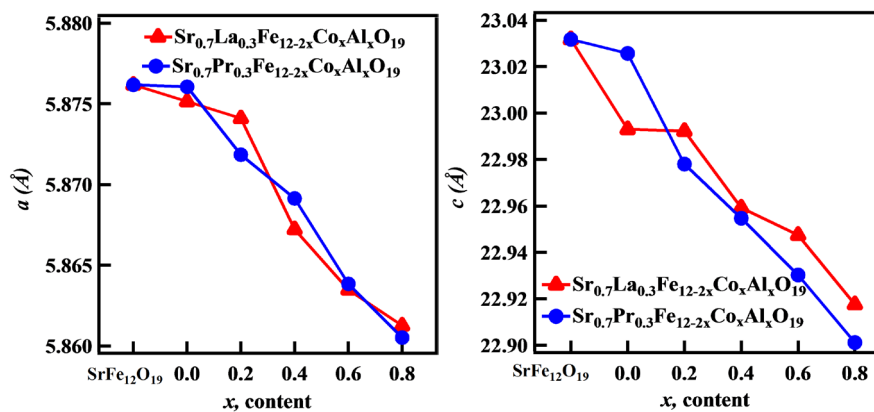


Figure 2. Lattice parameters of $\text{Sr}_{0.7}\text{La}_{0.3}\text{Fe}_{12-2x}\text{Co}_x\text{Al}_x\text{O}_{19}$ and $\text{Sr}_{0.7}\text{Pr}_{0.3}\text{Fe}_{12-2x}\text{Co}_x\text{Al}_x\text{O}_{19}$ as a function of content, x , derived from X-ray diffraction pattern.

Table 2. Lattice parameters of $\text{SrFe}_{12}\text{O}_{19}$, $\text{Sr}_{0.7}\text{La}_{0.3}\text{Fe}_{12-2x}\text{Co}_x\text{Al}_x\text{O}_{19}$ and $\text{Sr}_{0.7}\text{Pr}_{0.3}\text{Fe}_{12-2x}\text{Co}_x\text{Al}_x\text{O}_{19}$, as obtained from XRD pattern using Equation (1) and crystalline size using Equation (2).

	a (Å)	c (Å)	V (Å ³)	c/a	Crystallite size (nm)
SrFe₁₂O₁₉	5.876	23.031	686.707	3.919	80.77
Sr_{0.7}La_{0.3}Fe_{12-2x}Co_xAl_xO₁₉					
x = 0.0	5.856	22.936	688.498	3.919	58.345
x = 0.2	5.869	22.995	686.086	3.913	65.900
x = 0.4	5.867	22.943	684.758	3.911	61.670
x = 0.6	5.860	22.964	682.798	3.910	59.465
x = 0.8	5.869	23.012	681.155	3.908	56.070
Sr_{0.7}Pr_{0.3}Fe_{12-2x}Co_xAl_xO₁₉					
x = 0.0	5.873	23.034	687.308	3.914	60.825
x = 0.2	5.923	23.076	687.038	3.914	76.640
x = 0.4	5.915	23.047	684.448	3.913	65.985
x = 0.6	5.911	23.027	683.225	3.914	67.210
x = 0.8	5.904	23.035	681.995	3.911	65.000

Co^{2+} ($r \sim 0.72$ Å) for Fe^{3+} ($r \sim 0.64$ Å) and smaller La^{3+} ($r \sim 1.172$ Å) and Pr^{3+} ($r \sim 1.13$ Å) for the Sr^{2+} ($r \sim 1.32$ Å) ions [31]. According to Wagner [32], an examination of c/a parameter ratio may be used to quantify the structure type, as the M-type (magnetoplumbite) structure can be assumed if the ratio is observed to be in the range 3.917 and 3.963. As per **Table 2**, the c/a ratios of as-prepared samples are in the range of 3.908 to 3.919, assuring that the as-prepared samples have maintained the M-type structure.

The crystallite size of as-synthesized particles was calculated using Scherrer's equation [33]:

$$D(hkl) = k\lambda/(\beta \cos \theta) \quad (2)$$

where k denotes the Scherrer constant ($k = 0.9$), λ is the wavelength of x-ray source ($\lambda = 0.154056$ nm), β is the full-width-half-maximum of a diffraction peak and θ is the diffraction angle. As listed in **Table 2**, the crystallite size of as-synthesized samples is in the range of 54 to 77 nm. In the comparison of the pure $\text{SrFe}_{12}\text{O}_{19}$ sample with a crystallite size of 80.7 nm, the doped compounds show reduced crystallite size. Grain refinement is usually observed in rare-earth and doped oxide compounds [34]. This grain refinement is reported to result from the 1) increased microstrain and defect density with substitution content and 2) diffusion of substituent element to the grain boundaries, the migration that restrains the grain growth by lowering down the grain growth mobility. If the retarding force generated is more than the driving force for the grain growth due to dopants, the movement of the grain boundary is impeded [35].

The room temperature hysteresis loops, M vs. H , of $\text{Sr}_{0.7}\text{RE}_{0.3}\text{Fe}_{12-2x}\text{Co}_x\text{Al}_x\text{O}_{19}$ are shown in **Figure 3**. The magnetic parameters viz. saturation magnetization, M_s , remanence, M_r , and coercivity, H_c were extracted from the hysteresis loops and are listed in **Table 3**. The M vs. H curves show hard ferrites behaviors with high coercivity. The magnetic properties have been changed significantly upon RE^{3+} and Co^{2+} - Al^{3+} substitution in $\text{Sr}_{0.7}\text{RE}_{0.3}\text{Fe}_{12-2x}\text{Co}_x\text{Al}_x\text{O}_{19}$ as compared to undoped ferrite $\text{SrFe}_{12}\text{O}_{19}$. The M_s value of Pr^{3+} -SrM is observed to have a maximum value of 86 emu/g for $x = 0.2$ but decreases with Co^{2+} - Al^{3+} content and achieves a minimum value of 65 emu/g for $x = 0.8$. However, in the case of La^{3+} -SrM, the M_s increases with x and attains a maximum value of 87 emu/g at $x = 0.8$. As compared to pure $\text{SrFe}_{12}\text{O}_{19}$, La^{3+} -SrM displays a noticeable 20% enhancement while Pr^{3+} -SrM shows a 10% reduction in the M_s value. The variation of M_r and M_s as a function of x content is shown in **Figure 4**. The value of M_r follows a trend similar to that of M_s . As explained in the Mossbauer section, for series of compounds shows the marked preference of Co^{2+} - Al^{3+} for the $2a$ site, a site with the spin-up moment. Despite the substitution of Co^{2+} - Al^{3+} at the $2a$ site with the up-spin moment, the magnetization of La^{3+} -SrM displayed a marked increase in the magnetization value with the substitution. A possible explanation for this observation is that the substitution of non-magnetic La^{3+} at the Sr^{2+} 1) could enhance hyperfine fields at $12k$ site due to strengthening in the Fe^{3+} - O^{2-} - Fe^{3+} superexchange interaction giving higher net magnetization. This increase in the hyperfine field of $12k$ site is evident from the Mossbauer analysis, and 2) may increase the spin canting at the near-neighbor $4f$ site (Sr^{2+} - $4f \sim 0.366$ nm), which results in a positive contribution to the overall magnetic moment. However, the possibility of Co^{2+} occupying a $4f$ site cannot be ignored, which increases the net positive moment per unit cell of the compound [36] [37]

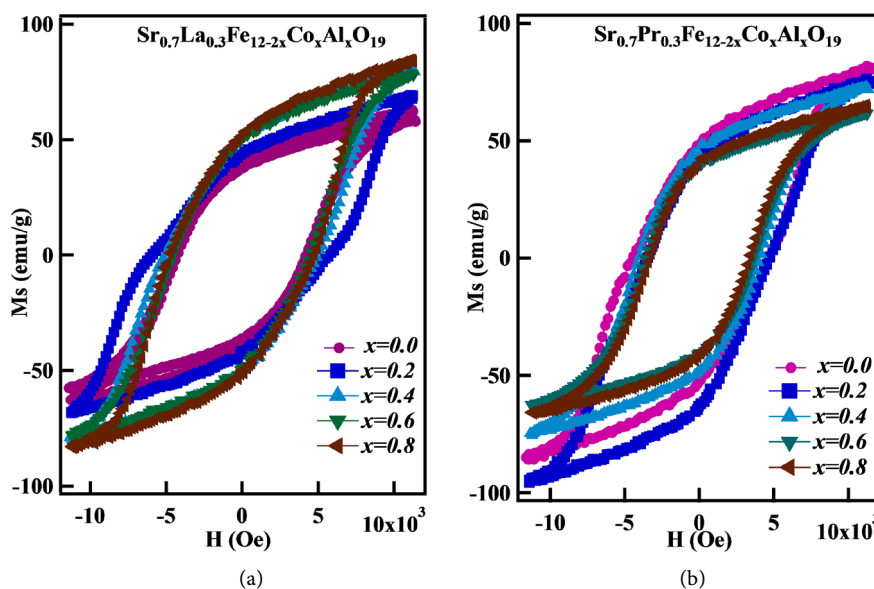
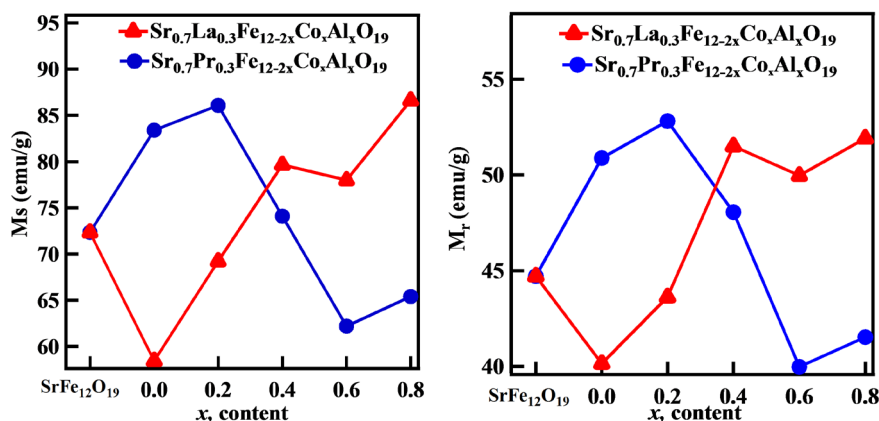


Figure 3. Room temperature VSM M vs. H loops of (a) $\text{Sr}_{0.7}\text{La}_{0.3}\text{Fe}_{12-2x}\text{Co}_x\text{Al}_x\text{O}_{19}$ and (b) $\text{Sr}_{0.7}\text{Pr}_{0.3}\text{Fe}_{12-2x}\text{Co}_x\text{Al}_x\text{O}_{19}$.

Table 3. Magnetic parameters of $\text{SrFe}_{12}\text{O}_{19}$, $\text{Sr}_{0.7}\text{La}_{0.3}\text{Fe}_{12-2x}\text{Co}_x\text{Al}_x\text{O}_{19}$ and $\text{Sr}_{0.7}\text{Pr}_{0.3}\text{Fe}_{12-2x}\text{Co}_x\text{Al}_x\text{O}_{19}$ measured using VSM. Curie temperature, T_c , of samples was measured using TGA.

	Ms (emu/g)	Mr (emu/g)	Mr/Ms	Hc (Oe)	Tc (°C)
SrFe₁₂O₁₉	72.35	44.71	0.61	3918	458.60
Sr_{0.7}La_{0.3}Fe_{12-2x}Co_xAl_xO₁₉					
$x = 0.0$	58.44	40.14	0.69	4318	477.80
$x = 0.2$	69.22	43.62	0.63	5829	427.13
$x = 0.4$	79.67	51.50	0.65	5031	506.00
$x = 0.6$	78.00	49.97	0.63	4498	492.38
$x = 0.8$	86.64	51.91	0.60	4761	455.75
Sr_{0.7}Pr_{0.3}Fe_{12-2x}Co_xAl_xO₁₉					
$x = 0.0$	83.40	50.88	0.61	4651	456.63
$x = 0.2$	86.09	52.81	0.61	4090	428.75
$x = 0.4$	74.10	48.05	0.65	4130	523.56
$x = 0.6$	62.20	39.97	0.64	3659	505.30
$x = 0.8$	65.40	41.52	0.63	3379	489.19

**Figure 4.** Room temperature Ms and Mr of $\text{Sr}_{0.7}\text{La}_{0.3}\text{Fe}_{12-2x}\text{Co}_x\text{Al}_x\text{O}_{19}$ and $\text{Sr}_{0.7}\text{Pr}_{0.3}\text{Fe}_{12-2x}\text{Co}_x\text{Al}_x\text{O}_{19}$ measured at 1.2 T field as a function of content, x .

[39]. On the other hand, the substitution of magnetic Pr^{3+} at the Sr^{2+} site may not allow spin-canting at the $4\bar{2}$ site, and with the replacement of Fe^{3+} at the $2a$ site, the overall magnetic moment decreases in the Pr^{3+} -SrM compounds.

The variation of coercivity, H_c , of La^{3+} -SrM and Pr^{3+} -SrM compounds as a function of x content is shown in **Figure 5**. Consistently La^{3+} -SrM samples display higher H_c values than Pr^{3+} -SrM compounds for all x values. The H_c value of La^{3+} -SrM displays a marked $\sim 50\%$ increase at $x = 0.2$ when compared to that of pure SrFe_{12}O ($H_c \sim 3918$ Oe). On the other hand, H_c value decreases linearly with increasing the x content for the Pr^{3+} -SrM compound. Being an extrinsic

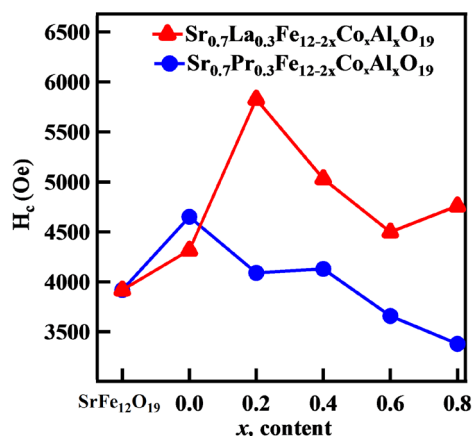


Figure 5. Coercivity, H_c , of $\text{Sr}_{0.7}\text{La}_{0.3}\text{Fe}_{12-2x}\text{Co}_x\text{Al}_x\text{O}_{19}$ and $\text{Sr}_{0.7}\text{Pr}_{0.3}\text{Fe}_{12-2x}\text{Co}_x\text{Al}_x\text{O}_{19}$ as a function of content, x .

property, the coercivity depends on factors such as crystal structure, morphological features, elemental composition, and defects. In general, H_c can be expressed as,

$$H_c = \left(\alpha \left(\frac{2K_1}{\mu_o M_s} \right) - N(M_r + M_s) \right) / \mu_o \quad (3)$$

where α is the microstructure factor which has a reciprocal dependence on the grain size, N is the demagnetization factor, $2K_1/(\mu_o M_s)$ is the H_a is the magnetocrystalline anisotropy field [39]. In the M-type hexaferrite, magnetocrystalline anisotropy mainly originates from Fe^{3+} ions at the $2b$ and $4f_1$ site [40] [41]. It has been reported that Al^{3+} ions have a preference for $4f_2$, $2a$, and $12k$ sites, [42] [43], and Co^{2+} ions mainly prefer $4f_2$ (mainly) and $2a$ sites [37] [38] [44]. In accordance with the Mossbauer analysis, discussed later, it is observed that in both series of samples studied herein, the Co^{3+} - Al^{3+} ions have a preference for the $2a$ site. Thus the intrinsic coercivity as per Equation (3), should increase for both series of samples due to the increase in the magnetocrystalline anisotropy, as the site $2b$ remains unaffected with the said substitution. However, from **Figure 5**, it is observed that the La^{3+} -SrM sample shows a maximum (5829 Oe) in coercivity value at $x = 0.2$, followed by a decrease with increasing x content in the sample. On the other hand, the H_c value of the Pr^{3+} -SrM sample shows a monotonous decrease with the x content in the sample. Also, the La^{3+} -SrM sample displays consistently higher coercive field value as compared to Pr^{3+} -SrM. In a comparative study on $\text{Sr}(\text{La}/\text{Pr})\text{Fe}_{12}\text{O}_{19}$ samples it was reported that the Pr^{3+} doped $\text{Sr}(\text{Pr})\text{Fe}_{12}\text{O}_{19}$ displayed higher coercivity than La^{3+} doped $\text{Sr}(\text{Pr})\text{Fe}_{12}\text{O}_{19}$ sample because of the higher magnetocrystalline anisotropy of the former. However, the contrary results in the present study can be explained by taking microstructure factor, α , in account in Equation (3) above. The La^{3+} -SrM samples have relatively smaller crystallite size as compared to Pr^{3+} -SrM; as a result, the microstructure factor, α , will have a higher value than that of Pr^{3+} -SrM sample. This will make the first term in the Equation (3) above greater than for La^{3+} -SrM as compared to that for Pr^{3+} -SrM. The observed decrease in coercivity with the substitution

could be attributed to the fact that the second term in the Equation (3) decreases much rapidly as compared to the αHa term.

The Curie temperature, T_c , of $\text{Sr}_{0.7}\text{RE}_{0.3}\text{Fe}_{12-2x}\text{Co}_x\text{Al}_x\text{O}_{19}$ are shown in **Figure 6**. The maximum T_c value for La^{3+} -SrM and Pr^{3+} -SrM was observed to be 505 and 525 K, respectively at $x = 0.40$. After attaining maximum value, the T_c decreases gradually for $x > 0.40$. The overall decrease in T_c after attaining maximum can be explained on the basis of three combined effects [45] [46], 1) substitution of Co^{2+} - Al^{3+} ions for Fe^{3+} ions reduce the Fe^{3+} ions and hence leads to a reduction of Fe^{3+} - O^{2-} - Fe^{3+} number of superexchange interaction and strength and 2) lattice contraction with the substitution alters the bond length and angle of Fe^{3+} - O^{2-} - Fe^{3+} from its optimum interaction strength value. However, in the beginning, T_c drops down for $x = 0.20$, where presumably Fe^{3+} might be substituted more with non-magnetic Al^{3+} and above combined effect become prevalent. However, the increasing magnetic Co^{2+} ion content helps regain the strength of the superexchange interaction and hence increases the T_c value for $x = 0.40$ [47].

In order to investigate the site occupancies of transition metal ions and resulting hyperfine parameters in the samples, Mossbauer spectra were collected at room temperature. **Figure 7** shows the fitted Mossbauer spectra as a function of content x in the as-synthesized samples. All spectra consist of five Lorentzian sextets originating from $12k$, $4f$, $4f$, $2a$, and $2b$ crystallographic sites of Fe^{3+} ions. The spectra were fitted with the constrain that all the linewidths of the absorption lines were the same. The extracted Mossbauer parameters are listed in **Table 4(a)** and **Table 4(b)**. The observed sequences of the magnetic hyperfine magnetic fields, HF ($4f > 2a > 4f > 12k > 2b$) and isomer shift, δ (the isomer shifts follow the sequence of $4f > 12k > 2a > 2b > 4f$) for both samples are in agreement with the reported results [47].

It is well known that the magnitude of the hyperfine magnetic field at the Fe^{3+} site depends on the distribution of neighboring magnetic cations. The hyperfine field, HF , the parameter of the most intense $12k$ line effectively shows no variation

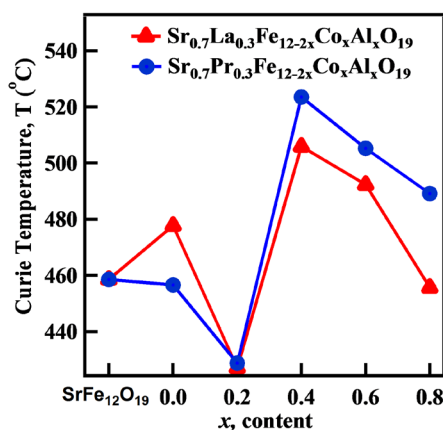
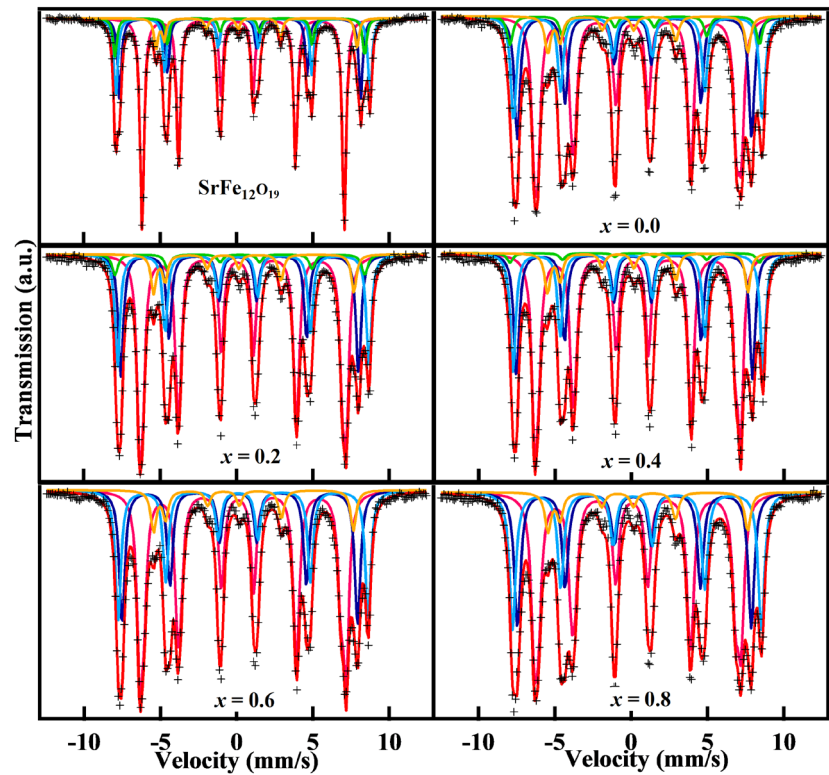
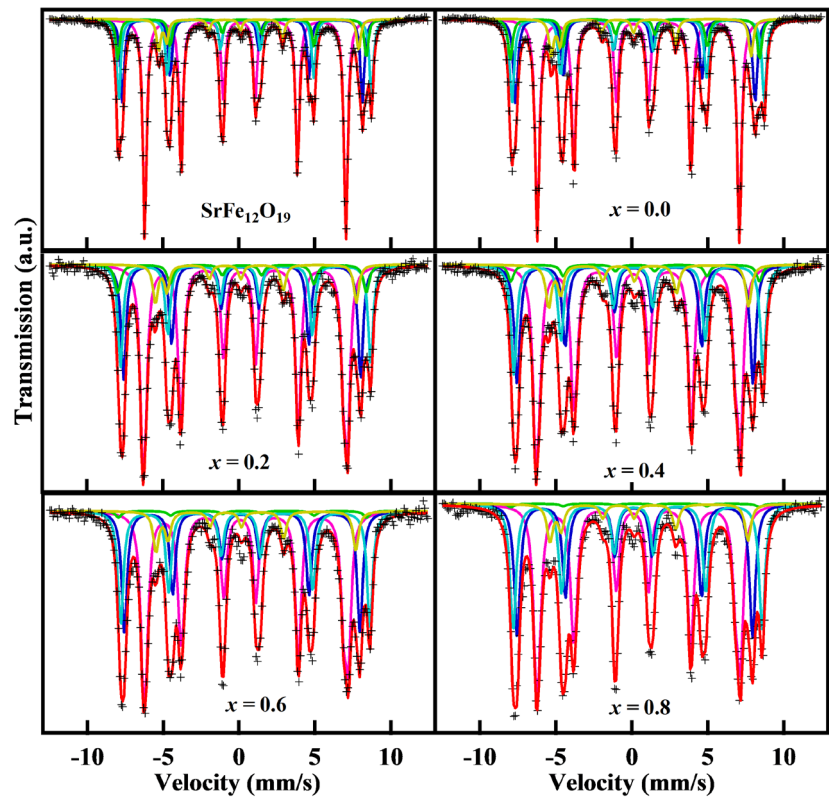


Figure 6. Curie temperature, T_c , of $\text{Sr}_{0.7}\text{La}_{0.3}\text{Fe}_{12-2x}\text{Co}_x\text{Al}_x\text{O}_{19}$ and $\text{Sr}_{0.7}\text{Pr}_{0.3}\text{Fe}_{12-2x}\text{Co}_x\text{Al}_x\text{O}_{19}$ as a function of content, x .



(a)



(b)

Figure 7. Room temperature fitted Mössbauer spectra of (a) $\text{Sr}_{0.7}\text{La}_{0.3}\text{Fe}_{12-2x}\text{Co}_x\text{Al}_x\text{O}_{19}$ and (b) $\text{Sr}_{0.7}\text{Pr}_{0.3}\text{Fe}_{12-2x}\text{Co}_x\text{Al}_x\text{O}_{19}$ respectively.

Table 4. (a) Hyperfine parameters of $\text{Sr}_{0.7}\text{La}_{0.3}\text{Fe}_{12-2x}\text{Co}_x\text{Al}_x\text{O}_{19}$ extracted from fitting room temperature Mossbauer spectra; (b) Hyperfine parameters of $\text{Sr}_{0.7}\text{Pr}_{0.3}\text{Fe}_{12-2x}\text{Co}_x\text{Al}_x\text{O}_{19}$ extracted from fitting room temperature Mossbauer spectra.

(a)					
$\text{Sr}_{0.7}\text{La}_{0.3}\text{Fe}_{12-2x}\text{Co}_x\text{Al}_x\text{O}_{19}$	x	HF (kOe)	QS (mm/s)	IS (mm/s)	Area (%)
12k (\uparrow)	SrFe ₁₂ O ₁₉	411.50	0.20	0.23	47.60
	0.0	413.52	0.18	0.23	44.23
	0.2	412.38	0.18	0.23	47.06
	0.4	413.66	0.17	0.23	46.97
	0.6	413.73	0.17	0.23	46.26
	0.8	416.37	0.18	0.24	43.50
4f1 (\downarrow)	SrFe ₁₂ O ₁₉	491.00	0.09	0.15	18.20
	0.0	477.73	0.05	0.15	23.20
	0.2	483.92	0.06	0.15	21.81
	0.4	480.87	0.06	0.15	22.72
	0.6	480.11	0.05	0.15	23.81
	0.8	475.82	0.05	0.16	24.63
4f2 (\downarrow)	SrFe ₁₂ O ₁₉	517.4	0.15	0.27	26.6
	0.0	507.18	0.17	0.26	20.05
	0.2	511.62	0.18	0.26	20.15
	0.4	509.46	0.18	0.26	21.37
	0.6	509.23	0.16	0.25	22.81
	0.8	506.32	0.14	0.25	24.90
2a (\uparrow)	SrFe ₁₂ O ₁₉	508.10	0.00	0.22	8.70
	0.0	508.10	0.00	0.22	5.60
	0.2	508.10	0.00	0.22	4.14
	0.4	508.10	0.00	0.22	1.84
	0.6	-	-	-	-
	0.8	-	-	-	-
2b (\uparrow)	SrFe ₁₂ O ₁₉	409.10	1.12	0.19	7.00
	0.0	407.55	0.98	0.10	6.92
	0.2	407.49	1.01	0.12	6.84
	0.4	408.37	0.97	0.10	7.10
	0.6	407.23	0.99	0.11	7.12
	0.8	406.20	0.99	0.11	6.98

(b)					
$\text{Sr}_{0.7}\text{Pr}_{0.3}\text{Fe}_{12-2x}\text{Co}_x\text{Al}_x\text{O}_{19}$	x	HF (kOe)	QS (mm/s)	IS (mm/s)	Area (%)
12k (↑)	SrFe ₁₂ O ₁₉	411.5	0.20	0.23	47.60
	0.0	413.4	0.20	0.24	46.70
	0.2	414.4	0.17	0.23	47.30
	0.4	413.4	0.16	0.23	46.20
	0.6	414.0	0.18	0.23	44.60
	0.8	412.3	0.19	0.22	42.50
4f (↓)	SrFe ₁₂ O ₁₉	491.0	0.09	0.15	18.20
	0.0	489.8	0.09	0.15	18.30
	0.2	485.0	0.06	0.16	21.10
	0.4	482.4	0.06	0.16	22.30
	0.6	482.8	0.04	0.16	23.60
	0.8	481.3	0.05	0.15	22.50
4f (↓)	SrFe ₁₂ O ₁₉	517.4	0.15	0.27	26.60
	0.0	516.0	0.15	0.27	18.10
	0.2	511.6	0.18	0.27	18.70
	0.4	510.2	0.18	0.26	20.40
	0.6	510.7	0.15	0.26	22.60
	0.8	509.6	0.13	0.26	24.50
2a (↑)	SrFe ₁₂ O ₁₉	508.1	0.00	0.22	8.70
	0.0	508.1	0.00	0.22	8.80
	0.2	508.1	0.00	0.22	5.90
	0.4	508.1	0.00	0.22	3.20
	0.6	508.1	0.00	0.22	1.30
	0.8	508.1	0.00	0.22	0.60
2b (↑)	SrFe ₁₂ O ₁₉	409.1	1.12	0.19	7.00
	0.0	408.4	1.10	0.17	8.10
	0.2	411.0	1.02	0.11	7.00
	0.4	408.9	0.99	0.12	7.80
	0.6	409.4	0.99	0.12	7.80
	0.8	405.0	1.01	0.12	7.00

with x in Pr^{3+} -SrM, while HF increases with x in the La^{3+} -SrM sample. The increase in HF value of La^{3+} -SrM is in agreement with the observed increase in the saturation magnetization, M_s , with content x . Other lines $4f1$, $2a$, and $4f2$ show a monotonous decrease in HF with x .

The isomer shift plot as a function of x is shown in **Figure 8**. The isomer shift, δ , for both series of samples for all sites visibly remains invariant except for the $2b$ site. Also, the $2b$ site's isomer shift value clearly reflects the influence of the

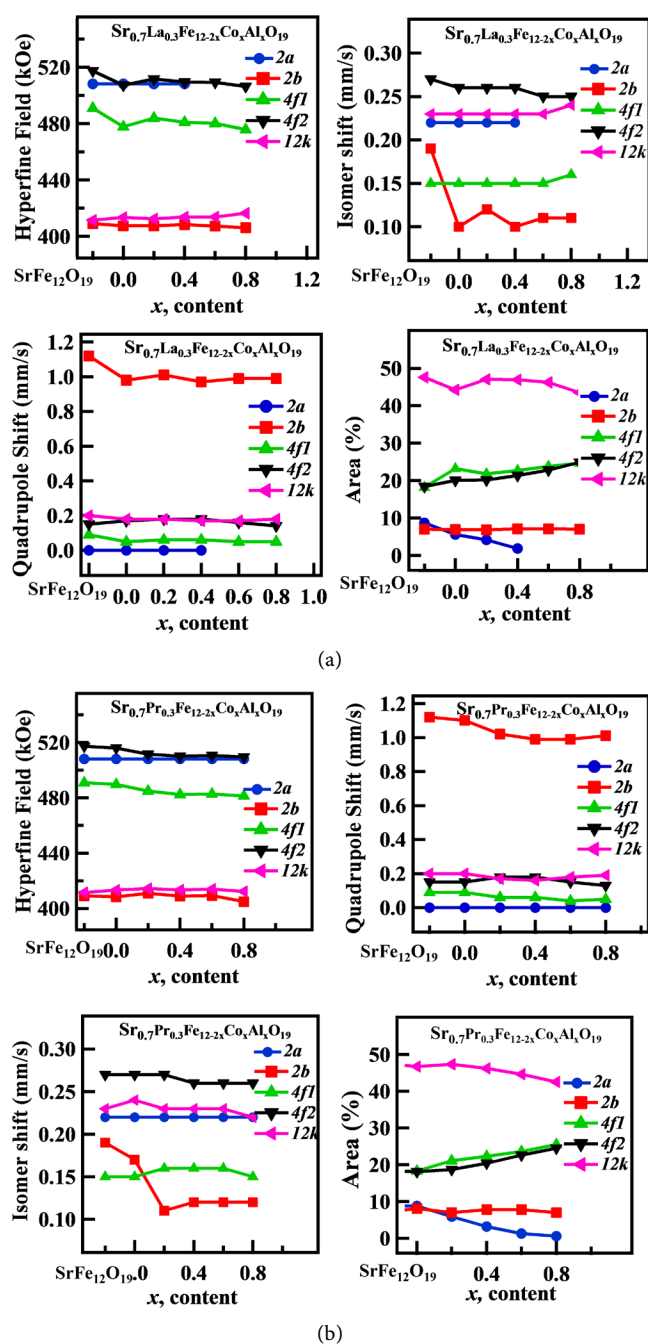


Figure 8. Room temperature hyperfine parameters of $\text{Sr}_{0.7}\text{La}_{0.3}\text{Fe}_{12-2x}\text{Co}_x\text{Al}_x\text{O}_{19}$ and $\text{Sr}_{0.7}\text{Pr}_{0.3}\text{Fe}_{12-2x}\text{Co}_x\text{Al}_x\text{O}_{19}$ obtained from Mossbauer spectral analysis.

rare-earth ion in the compound. In the presence of rare-earth ion, the isomer shift value of $2b$ drops significantly as compared to that of a pure $\text{SrFe}_{12}\text{O}_{19}$ compound. Isomer shift is a measure of $3d$ electron density at the nucleus of the Fe atom. The closest sites of Sr^{2+} sites are $12k$, $4f$, and $2b$. The $2b$ sites are located in the same plane as Sr^{2+} ions (at a distance of 0.340 nm), while the $4f$ and $12k$ sites are located in the adjacent planes at nearly the same distance from Sr^{2+} viz. Sr^{2+} - $12k \sim 0.365$ nm and Sr^{2+} - $4f \sim 0.366$ nm [48] [49]. Pr [Xe] $4f^3 6s^2$ and La[Xe] $5d^1 6s^2$ with more electrons as compared to Sr (Kr[$5s^2$]) has a negative effect on the isomer shift, that is increased substitution of Pr^{3+} or La^{3+} increases the net s -electron charge density at the $2b$ site, which in turn decreases the isomer shift value at the $2b$ site.

The quadrupole shift, QS, values of $2b$ site show a similar $\sim 10\%$ drop in both Pr^{3+} and La^{3+} substituted samples. The quadrupole values for all sites remain invariant with x for both series of samples. It is known that QS is a measure of the asymmetry of a crystallographic site. Since the $2b$ sites are located in the same plane as Sr^{2+} , the substitution of the smaller Pr^{3+} and La^{3+} for Sr^{2+} ions induces a deformation, which affects the electronic site symmetry of the nearby $2b$ site. Due to the substitution of smaller La^{3+} and Pr^{3+} ion for Sr^{2+} ion, the lattice constant c contracts. Consequently, large Fe-O distances parallel to the c -axis decreases. As a result, the oxygen bipyramid of the $2b$ -site becomes more symmetric, which is in agreement with the observed reduction in the quadrupole shift value with content x . A similar decrease in $2b$ quadrupole splitting originating from the presence of La^{3+} substitution has been reported in $\text{Sr}_{1-x}\text{La}_x\text{Fe}_{12-y}\text{Co}_y\text{O}_{19}$ [39].

A close examination of the fitted spectra shows a decreasing trend of $2a$ absorption intensities with increasing x . Without Co^{2+} - Al^{3+} co-doping, the intensity of $2a$ site lines in both $\text{Sr}_{0.7}\text{La}_{0.3}\text{Fe}_{12}\text{O}_{19}$ and $\text{Sr}_{0.7}\text{Pr}_{0.3}\text{Fe}_{12}\text{O}_{19}$ are nearly the same as that of undoped $\text{SrFe}_{12}\text{O}_{19}$. However, with the substitution of Co^{2+} - Al^3 , the $2a$ absorption area decreased linearly and finally disappeared at $x = 0.6$ and 1.0 for La^{3+} -SrM and Pr^{3+} -SrM sample, respectively. This suggests preferential occupation of Co^{2+} - Al^3 for the $2a$ site. It has already been reported that Al^{3+} ion prefers $12k$ and $2a$ site [50] while Co^{2+} was reported to enter $4f$ site in $\text{Sr}_{1-x}\text{La}_x\text{Fe}_{12-x}\text{Co}_x\text{O}_{19}$ [51]. There is only one $2a$ site in every one formula unit of M-type hexaferrite. Therefore, the fact that the $2a$ absorption line of $\text{Sr}_{0.7}\text{La}_{0.3}\text{Fe}_{12-2x}\text{Co}_x\text{Al}_x\text{O}_{19}$ disappeared completely at $x = 0.6$ means that all the Co^{2+} - Al^3 dopants almost exclusively go into $2a$ site. In the case when $x > 0.5$, the excessive Co^{2+} - Al^3 dopant should occupy the crystallographic sites other than the $2a$ site. On the other hand, in the case of $\text{Sr}_{0.7}\text{Pr}_{0.3}\text{Fe}_{12-2x}\text{Co}_x\text{Al}_x\text{O}_{19}$, $2a$ absorption intensity has decreased linearly and has completely diminished at $x = 1.0$, which indicates that all the $2a$ sites become full when $x = 1.0$. This suggests that only half of the Co^{2+} - Al^{3+} dopant occupies the $2a$ site compared to the case of the La^{3+} -SrM sample. Then, the other half of the $2a$ site should be occupied by Fe^{3+} ions through the range of x examined. In the case of Pr^{3+} series samples, a slight decline in the absorption area

for the most intense $12k$ site is observed, while in the La^{3+} containing samples, $12k$ areal almost remains constant. Thus it seems that the excessive $\text{Co}^{2+}\text{-Al}^{3+}$ dopant occupies the $2a$ site and $12k$ site in $\text{Sr}_{0.7}\text{Pr}_{0.3}\text{Fe}_{12-2x}\text{Co}_x\text{Al}_x\text{O}_{19}$. The above observation clearly indicates that the tendency of $12k$ site occupation by the $\text{Co}^{2+}\text{-Al}^{3+}$ dopant is affected by the species of rare-earth ions at the Sr^{2+} site. Where $\text{Co}^{2+}\text{-Al}^{3+}$ impurity mostly prefers $2a$ site and its preference for $12k$ site is enhanced in the presence of Pr^{3+} rather than La^{3+} , once the $2a$ site is completely filled. This observation is interesting considering the fact that there are no $2a$ sites in the vicinity of Sr^{2+} , and hence the substitution at Sr^{2+} with rare-earth ions is not expected to influence the site occupancy at the $2a$ site. Furthermore, the physical reason for the preferential site occupancy of $\text{Co}^{2+}\text{-Al}^{3+}$ in the presence of La^{3+} or Pr^{3+} is not clear at this stage. Mossbauer spectroscopy cannot discriminate against the site occupancies of both Co^{2+} and Al^{3+} ions separately. But one scenario is that Co^{2+} ions might not prefer the $2a$ site in the presence of Pr^{3+} ion, which needs further investigation.

4. Conclusion

The structural, magnetic, and Mossbauer spectrum study of the influence of rare-earth La^{3+} and Pr^{3+} on $\text{Sr}_{0.7}\text{RE}_{0.3}\text{Fe}_{12-2x}\text{Co}_x\text{Al}_x\text{O}_{19}$ (RE: La and Pr) hexaferrite compounds were investigated. Overall, dopant ion brings a unit cell contraction, which affects the Curie temperature and saturation magnetization of both series of samples. $\text{La}^{3+}\text{-SrM}$ samples show marked improvement in the magnetization value, while $\text{Pr}^{3+}\text{-SrM}$ samples show deterioration in M_s value with the $\text{Co}^{2+}\text{-Al}^{3+}$ substitution. This is suggestive of the fact that magnetic Pr^{3+} , unlike non-magnetic La^{3+} (no $4f$ electrons), substitution for Sr^{2+} could be detrimental to the overall magnetization behavior of the $\text{SrFe}_{12}\text{O}_{19}$ compound. The $\text{Co}^{2+}\text{-Al}^{3+}$ substitution brings in grain refinement, more for the $\text{La}^{3+}\text{-SrM}$ than $\text{Pr}^{3+}\text{-SrM}$, which has a considerable impact on the coercivity values of the compound. The Mossbauer spectral analysis revealed $2a$ as a preferred substitution for $\text{Co}^{2+}\text{-Al}^{3+}$ ions for both series of samples. Due to lattice contraction, the $2b$ site displayed a considerable reduction in its quadrupole shift value. The improved hyperfine field for the $12k$ site in the $\text{La}^{3+}\text{-SrM}$ series is attributed to the increase in its magnetization value with the substitution of $\text{Co}^{2+}\text{-Al}^{3+}$ ions for Fe^{3+} . For the study, it is concluded that the substitution of rare-earth ions with $4f$ charge distribution for Sr^{2+} could be detrimental to the overall magnetic performance of the M-type hexaferrite materials.

Conflicts of Interest

The authors declare no conflicts of interest regarding the publication of this paper.

References

- [1] Chen, N., Yang, K. and Mingyuan, G. (2010) Microwave Absorption Properties of

- La-Substituted M-Type Strontium Ferrites. *Journal of Alloys and Compounds*, **490**, 609-612. <https://doi.org/10.1016/j.jallcom.2009.10.116>
- [2] Riches, E.E. (1972) Ferrites: A Review of Materials and Applications. 3rd Edition, Mills & Boon, Richmond.
- [3] Chin, T.-S. (2000) Permanent Magnet Films for Applications in Microelectromechanical Systems. *Journal of Magnetism and Magnetic Materials*, **209**, 75-79. [https://doi.org/10.1016/S0304-8853\(99\)00649-6](https://doi.org/10.1016/S0304-8853(99)00649-6)
- [4] Hernandez, P., De Francisco, C., Munoz, J.M., Iniguez, J., Torres, L. and Zazo, M. (1996) Influence of Sintering Atmosphere on the Magnetic After-Effect in Strontium Ferrites. *Journal of Magnetism and Magnetic Materials*, **157-158**, 123-124. [https://doi.org/10.1016/0304-8853\(95\)01070-X](https://doi.org/10.1016/0304-8853(95)01070-X)
- [5] Jin, Z.Q., Tang, W., Zhang, J.R., Lin, H. and Du, Y.W. (1998) Magnetic Properties of Isotropic SrFe₁₂O₁₉ Fine Particles Prepared by Mechanical Alloying. *Journal of Magnetism and Magnetic Materials*, **182**, 231-237. [https://doi.org/10.1016/S0304-8853\(97\)00679-3](https://doi.org/10.1016/S0304-8853(97)00679-3)
- [6] Qiao, L., You, L., Zheng, J., Jiang, L. and Sheng, J. (2007) The Magnetic Properties of Strontium Hexaferrites with La-Cu Substitution Prepared by SHS Method. *Journal of Magnetism and Magnetic Materials*, **318**, 74-78. <https://doi.org/10.1016/j.jmmm.2007.04.028>
- [7] Beseničar, S. and Miha, D. (1991) High Coercivity Sr Hexaferrites. *Journal of Magnetism and Magnetic Material*, **101**, 307-309. [https://doi.org/10.1016/0304-8853\(91\)90763-Z](https://doi.org/10.1016/0304-8853(91)90763-Z)
- [8] Rezlescu, L., Rezlescu, E., Popa, P.D. and Rezlescu, N. (1999) Fine Barium Hexaferrite Powder Prepared by the Crystallization of Glass. *Journal of Magnetism and Magnetic Materials*, **193**, 288-290. [https://doi.org/10.1016/S0304-8853\(98\)00442-9](https://doi.org/10.1016/S0304-8853(98)00442-9)
- [9] Zhong, W., Ding, W.P., Zhang, N., Hong, J.M., Yan, Q.J. and Du, Y.W. (1997) Key Step in Synthesis of Ultrafine BaFe₁₂O₁₉ by Sol-Gel Technique. *Journal of Magnetism and Magnetic Materials*, **168**, 196-202. [https://doi.org/10.1016/S0304-8853\(96\)00664-6](https://doi.org/10.1016/S0304-8853(96)00664-6)
- [10] Kojima, H. (1982) Chapter 5. Fundamental Properties of Hexagonal Ferrites with Magnetoplumbite Structure. In: *Handbook of Ferromagnetic Materials*, Elsevier, Amsterdam, Vol. 3, 305-391. [https://doi.org/10.1016/S1574-9304\(05\)80091-4](https://doi.org/10.1016/S1574-9304(05)80091-4)
- [11] Luo, H., Rai, B.K., Mishra, S.R., Nguyen, N.N. and Liu, J.P. (2012) Physical and Magnetic Properties of Highly Aluminum Doped Strontium Ferrite Nanoparticles Prepared by Auto-Combustion Route. *Journal of Magnetism and Magnetic Materials*, **324**, 2602-2608. <https://doi.org/10.1016/j.jmmm.2012.02.106>
- [12] Shirtcliffe, N.J., Thompson, S., O'keefe, E.S. Appleton, S. and Perry, C.C. (2007) Highly Aluminium Doped Barium and Strontium Ferrite Nanoparticles Prepared by Citrate Auto-Combustion Synthesis. *Materials Research Bulletin*, **42**, 281-287. <https://doi.org/10.1016/j.materresbull.2006.06.001>
- [13] Fang, Q.Q., Liu, Y.M., Yin, P. and Li, X.G. (2001) Magnetic Properties and Formation of Sr Ferrite Nanoparticle and Zn, Ti/Ir Substituted Phases. *Journal of Magnetism and Magnetic Materials*, **234**, 366-370. [https://doi.org/10.1016/S0304-8853\(01\)00428-0](https://doi.org/10.1016/S0304-8853(01)00428-0)
- [14] Iqbal, M.J., Ashiq, M.N., Gomes, P.H. and Munoz, J.M. (2008) Synthesis, Physical, Magnetic and Electrical Properties of Al-Ga Substituted Co-Precipitated Nanocrystalline Strontium Hexaferrite. *Journal of Magnetism and Magnetic Materials*, **320**, 881-886. <https://doi.org/10.1016/j.jmmm.2007.09.005>

- [15] Albanese, G., Carbuicchio, M. and Deriu, A. (1974) Temperature Dependence of the Sublattice Magnetizations in Al- and Ga-Substituted M-Type Hexagonal Ferrites. *Physica Status Solidi*, **23**, 351-358. <https://doi.org/10.1002/pssa.2210230202>
- [16] Ashiqa, M.N., Iqbal, M.J. and Gul, I.H. (2009) Structural, Magnetic and Dielectric Properties of Zr-Cd Substituted Strontium Hexaferrite (SrFe₁₂O₁₉) Nanoparticles. *Journal of Alloys and Compounds*, **487**, 341-345. <https://doi.org/10.1016/j.jallcom.2009.07.140>
- [17] Le Breton, J.M., Teillet, J., Wiesinger, G., Morel, A., Kools, F. and Tenaud, P. (2002) Mossbauer Investigation of Sr-Fe-O Hexaferrites with La-Co Addition. *IEEE Transactions on Magnetics*, **38**, 2952-2954. <https://doi.org/10.1109/TMAG.2002.803177>
- [18] Nourbakhsh, A.A., Noorbakhsh, M., Nourbakhsh, M., Shaygan, M. and Mackenzie, K.J.D. (2011) The Effect of Nano Sized SrFe₁₂O₁₉ Additions on the Magnetic Properties of Chromium-Doped Strontium-Hexaferrite Ceramics. *Journal of Materials Science: Materials in Electronics*, **22**, 1297-1302. <https://doi.org/10.1007/s10854-011-0303-3>
- [19] Liu, X.S., Zhong, W., Yang, S., Yu, Z., Gu, B.X. and Du, Y. (2002) Structure and Magnetic Properties of La³⁺-Substituted Strontium Hexaferrite Particles Prepared by Sol-Gel Method. *Physica Status Solidi*, **193**, 314-319. [https://doi.org/10.1002/1521-396X\(200209\)193:2<314::AID-PSSA314>3.0.CO;2-W](https://doi.org/10.1002/1521-396X(200209)193:2<314::AID-PSSA314>3.0.CO;2-W)
- [20] Dahal, J.N., Neupane, D. and Mishra, S.R. (2019) Exchange-Coupling Behavior in SrFe₁₂O₁₉/La_{0.7}Sr_{0.3}Mn_{0.3} Nanocomposites. *Ceramics*, **2**, 100-111. <https://doi.org/10.3390/ceramics2010010>
- [21] Mocuta, H., Lechevallier, L., Le Breton, J.M., Wang, J.F. and Harris, I.R. (2004) Structural and Magnetic Properties of Hydrothermally Synthesised Sr_{1-x}Nd_xFe₁₂O₁₉ Hexagonal Ferrites. *Journal of Alloys and Compounds*, **364**, 48-52. [https://doi.org/10.1016/S0925-8388\(03\)00545-0](https://doi.org/10.1016/S0925-8388(03)00545-0)
- [22] Lechevallier, L., Le Breton, J.M., Wang, J.F. and Harris, I.R. (2004) Structural and Magnetic Properties of Hydrothermally Synthesised Sr_{1-x}Nd_xFe₁₂O₁₉ Hexagonal Ferrites. *Journal of Magnetism and Magnetic Materials*, **269**, 192-196. [https://doi.org/10.1016/S0304-8853\(03\)00591-2](https://doi.org/10.1016/S0304-8853(03)00591-2)
- [23] Wang, J.F., Ponton, C.B. and Harris, I.R. (2001) A Study of the Magnetic Properties of Hydrothermally Synthesised Sr Hexaferrite with Sm Substitution. *Journal of Magnetism and Magnetic Materials*, **234**, 233-240. [https://doi.org/10.1016/S0304-8853\(01\)00366-3](https://doi.org/10.1016/S0304-8853(01)00366-3)
- [24] Lechevallier, L., Le Breton, J.M., Morel, A. and Tenaud, P. (2008) On the Solubility of Rare Earths in M-Type SrFe₁₂O₁₉ Hexaferrite Compounds. *Journal of Physics: Condensed Matter*, **20**, Article ID: 175203. <https://doi.org/10.1088/0953-8984/20/17/175203>
- [25] Polyko, D.D., Bashkurov, L.A., Trukhanov, S.V., Lobanovskii, L.S. and Sirota, I.M. (2011) Crystal Structure and Magnetic Properties of High-Coercivity Sr_{1-x}Pr_xFe_{12-x}Zn_xO₁₉ Solid Solutions. *Inorganic Materials*, **47**, 77-79. <https://doi.org/10.1134/S0020168511010110>
- [26] Yang, Y.J. and Liu, X.S. (2014) Microstructure and Magnetic Properties of La-Cu Doped M-Type Strontium Ferrites Prepared by Ceramic Process. *Materials Technology*, **29**, 232-236.
- [27] Corral Huacuz, J.C. and Mendoza-Suárez, G. (2002) Preparation and Magnetic Properties of Ir-Co and La-Zn Substituted Barium Ferrite Powders Obtained by Sol-Gel. *Journal of Magnetism and Magnetic Materials*, **430**, 430-433.

- [https://doi.org/10.1016/S0304-8853\(01\)01141-6](https://doi.org/10.1016/S0304-8853(01)01141-6)
- [28] Torkian, S., Ghasemi, A., Shojarazavi, R. and Tavoosi, M. (2016) Structural and Magnetic Properties of High Coercive Al-Substituted Strontium Hexaferrite Nanoparticles. *Journal of Superconductivity and Novel Magnetism*, **29**, 1627-1640. <https://doi.org/10.1007/s10948-016-3450-1>
- [29] Trusov, L.A., Gorbachev, E.A., Lebedev, V.A., Sleptsova, A.E., Roslyakov, I.V., Kozlyakova, E.S., Vasiliev, A.V., Dinnebier, R.E. Jansen, M. and Kazin, P.E. (2018) Ca-Al Double-Substituted Strontium Hexaferrites with Giant Coercivity, *Chemical Communications*, **54**, 479-482. <https://doi.org/10.1039/C7CC08675J>
- [30] Narang, S.B., Singh, A. and Singh, K. (2014) High Frequency Dielectric Behavior of Rare Earth Substituted Sr-M Hexaferrite. *Journal of Ceramic Processing Research*, **8**, 347.
- [31] Shannon, R.D. (1976) Revised Effective Ionic Radii and Systematic Studies of Interatomic Distances in Halides and Chalcogenides. *Acta Crystallographica*, **A32**, 751-767. <https://doi.org/10.1107/S0567739476001551>
- [32] Wagner, T.R. (1998) Preparation and Crystal Structure Analysis of Magnetoplumbite-Type $\text{Ba}_{12}\text{O}_{19}$, *Journal of Solid State Chemistry*, **136**, 120-124. <https://doi.org/10.1006/jssc.1997.7681>
- [33] Cullity, B.D. (1956) Elements of X-Ray Diffraction. 2nd Edition, Addison-Wesley Publishing, Boston.
- [34] Dahal, J.N., Wang, L., Mishra, S.R., Nguyen, V.V., and Liu, J.P. (2014) Synthesis and Magnetic Properties of $\text{SrFe}_{12-x}\text{Al}_x\text{Co}_y\text{O}_{19}$ Nanocomposites Prepared via Auto-combustion Technique. *Journal of Alloys and Compounds*, **595**, 213-220. <https://doi.org/10.1016/j.jallcom.2013.12.186>
- [35] Zi, Z.F., Sun, Y.P., Zhu, X.B., Yang, Z.R. and Song, W.H. (2008) Structural and Magnetic Properties of $\text{SrFe}_{12}\text{O}_{19}$ Hexaferrite Synthesized by a Modified Chemical Co-Precipitation Method. *Journal of Magnetism and Magnetic Materials*, **320**, 2746-2751. <https://doi.org/10.1016/j.jmmm.2008.06.009>
- [36] Wiesinger, G., Muller, M., Grossinger, R., Pieper, M., Morel, A., Kools, F., Tenad, P., Le Breton, J.M. and Kreisel, J. (2002) Substituted Ferrites Studied by Nuclear Methods. *Physica Status Solidi*, **189**, 499-508. [https://doi.org/10.1002/1521-396X\(200202\)189:2<499::AID-PSSA499>3.0.CO;2-H](https://doi.org/10.1002/1521-396X(200202)189:2<499::AID-PSSA499>3.0.CO;2-H)
- [37] Lechevallier, L., Le Breton, J.M., Teillet, J. Morel, A., Kools, F. and Tenaud, P. (2003) Mössbauer Investigation of $\text{Sr}_{1-x}\text{La}_x\text{Fe}_{12-y}\text{Co}_y\text{O}_{19}$ Ferrites. *Physica B: Condensed Matter*, **327**, 135-139. [https://doi.org/10.1016/S0921-4526\(02\)01712-X](https://doi.org/10.1016/S0921-4526(02)01712-X)
- [38] Le Breton, J.-M., Teillet, J., Wiesinger, G., Morel, A., Kools, F. and Tenaud, P. (2002) Mossbauer Investigation of Sr-Fe-O Hexaferrites La-Co Addition. *IEEE Transactions on Magnetics*, **38**, 2952-2954. <https://doi.org/10.1109/TMAG.2002.803177>
- [39] Kools, F. ((1985) Factors Governing the Coercivity of Sintered Anisotropic M Type Ferrite. *Le Journal de Physique Colloques*, **46**, 346-349.
- [40] Zhou, X.Z., Morrish, A.H., Li, Z.W. and Hong, Y.K. (1991) Site Preference for Co^{2+} and Ti^{4+} in Co-Ti Substituted Barium Ferrites. *IEEE Transactions on Magnetics*, **27**, 4654-4656. <https://doi.org/10.1109/20.278906>
- [41] Han, D.H., Yang, Z., Zeng, H.X., Zhou, X.Z. and Morrish, A.H. (1994) Cation Site Preference and Magnetic Properties of Co-Sn-Substituted Ba Ferrites Particles. *Journal of Magnetism and Magnetic Materials*, **137**, 191-196. [https://doi.org/10.1016/0304-8853\(94\)90205-4](https://doi.org/10.1016/0304-8853(94)90205-4)

- [42] Choi, D.H., An, S.Y., Lee, S.W., Shim, I.-B. and Kim, C.S. (2004) Site Occupancy and Anisotropy Distribution of Al Substituted Ba-Ferrite with High Coercivity. *Physica State Solid*, **241**, 1736-1739. <https://doi.org/10.1002/pssb.200304633>
- [43] Albanese, G. (1995) Mossbauer Investigation of Aluminium Substituted Barium Hexaferrites in the Paramagnetic State. *Journal of Magnetism and Magnetic Materials*, **147**, 421-426. [https://doi.org/10.1016/0304-8853\(95\)00063-1](https://doi.org/10.1016/0304-8853(95)00063-1)
- [44] Lechevallier, L., Le Breton, J.M., Morel, A. and Tenaud, P. (2007) Influence of the Presence of Co on the Rare Earth Solubility in M-Type Hexaferrite Powders. *Journal of Magnetism and Magnetic Materials*, **316**, e109-e111. <https://doi.org/10.1016/j.jmmm.2007.02.042>
- [45] Ghimire, M., Yoon, S., Wang, S.L., Neupane, D., Alam, J. and Mishra, S.R. (2018) Influence of La Content on Magnetic Properties of Cu Doped M-Type Strontium Hexaferrite: Structural, Magnetic, and Mossbauer Spectroscopy Study. *Journal of Magnetism and Magnetic Materials*, **454**, 110-120. <https://doi.org/10.1016/j.jmmm.2018.01.062>
- [46] Kunwar, D.L., Neupane, D., Dahal, J.N. and Mishra, S.R. (2019) Structural, Magnetic, and Electrical Properties of Re Doped $\text{Sr}_{0.82}\text{Re}_{0.18}\text{Fe}_{12-x}\text{Al}_x\text{O}_{19}$ (Re = Gd, Pr, Sm) Compound. *Advances in Materials Physics and Chemistry*, **9**, 175. <https://doi.org/10.4236/ampc.2019.99014>
- [47] Evans, B.J., Grandjean, F., Lilot, A.P., Vogel, R.H. and Gerard, A. (1987) ^{57}Fe Hyperfine Interaction Parameters and Selected Magnetic Properties of High Purity $\text{MFe}_{12}\text{O}_{19}$ (M = Sr, Ba). *Journal of Magnetism and Magnetic Materials*, **67**, 123-129. [https://doi.org/10.1016/0304-8853\(87\)90728-1](https://doi.org/10.1016/0304-8853(87)90728-1)
- [48] Wartewig, P., Krause, M.K., Esquinazi, P., Rösler, S. and Sonntag, R. (1999) Magnetic Properties of Zn- and Ti-Substituted Barium Hexaferrite. *Journal of Magnetism and Magnetic Materials*, **192**, 83-99. [https://doi.org/10.1016/S0304-8853\(98\)00382-5](https://doi.org/10.1016/S0304-8853(98)00382-5)
- [49] Obradors, X., Solans, X.A., Collomb, D., Samaras, J., Rodriguez, M., Pernet, M. and Font-Altaba, M. (1988) Crystal Structure of Strontium Hexaferrite $\text{SrFe}_{12}\text{O}_{19}$. *Journal of Solid State Chemistry*, **72**, 218-224. [https://doi.org/10.1016/0022-4596\(88\)90025-4](https://doi.org/10.1016/0022-4596(88)90025-4)
- [50] Dixit, V., Nandadasa, C.N., Kim, S.G., Kim, S., Park, J., Hong, Y.K. and Moitra, A. (2015) Site Occupancy and Magnetic Properties of Al-Substituted M-Type Strontium Hexaferrite. *Journal of Applied Physics*, **117**, Article ID: 243904. <https://doi.org/10.1063/1.4922867>
- [51] Lechevallier, L. and Le Breton, J.M. (2005) Substitution Effects in M-Type Hexaferrite Powders Investigated by Mössbauer Spectrometry. *Journal of Magnetism and Magnetic Materials*, **290**, 1237-1239. <https://doi.org/10.1016/j.jmmm.2004.11.411>